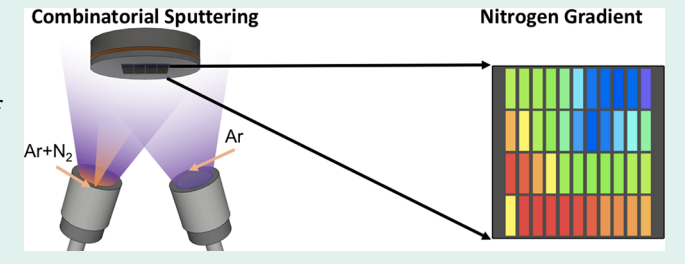


Combinatorial Nitrogen Gradients in Sputtered Thin Films

Yanbing Han,*,†,‡® Bethany Matthews,‡,§ Dennice Roberts,‡,|| Kevin R. Talley,‡,⊥ Sage R. Bauers,‡ Craig Perkins, [‡] Qun Zhang, [†] and Andriy Zakutayev*, [‡]

Supporting Information

ABSTRACT: High-throughput synthesis and characterization methods can significantly accelerate the rate of experimental research. For physical vapor deposition (PVD), these methods include combinatorial sputtering with intentional gradients of metal/metalloid composition, temperature, and thickness across the substrate. However, many other synthesis parameters still remain out of reach for combinatorial methods. Here, we extend combinatorial sputtering parameters to include gradients of gaseous elements in thin films.



Specifically, a nitrogen gradient was generated in a thin film sample library by placing two MnTe sputtering sources with different gas flows (Ar and Ar/N₂) opposite of one another during the synthesis. The nitrogen content gradient was measured along the sample surface, correlating with the distance from the nitrogen source. The phase, composition, and optoelectronic properties of the resulting thin films change as a function of the nitrogen content. This work shows that gradients of gaseous elements can be generated in thin films synthesized by sputtering, expanding the boundaries of combinatorial science.

KEYWORDS: physical vapor deposition, high-throughput experiments, spatially resolved characterization, thin film, combinatorial sputtering

INTRODUCTION

Combinatorial thin film deposition techniques and related spatially resolved characterization enable new high throughput experimental insights into novel and existing material systems. 1-3 Through manipulation of various experimental conditions during physical vapor deposition (PVD), combinatorial techniques have demonstrated gradients in metal/ metalloid composition,^{4,5} substrate temperature,^{6,7} and film thickness,8 such that a single synthesis can produce many different samples. However, few reports exist concerning the effects of atmospheric gas gradients in the PVD environment. Inhomogeneity in the surrounding gas environment has the potential for non-negligible effects on material composition, structure, and properties. This is particularly important in combinatorial sputtering chambers that rely on fixed metallic sources and substrate positions to create the appropriate gradient.

Directional control of vapor phase constituents in thin film deposition processes has been previously demonstrated in metal organic chemical vapor deposition (MOCVD).9 By manipulating the spatial arrangement of different gaseous precursor sources, one can generate a composition gradient within vanadium oxynitride thin films for combinatorial syntheses. 10 Besides, gradients in gas phase transport during annealing have been reported to have a significant effect on the efficiency of photovoltaic devices with chalcogenide absorber materials such as CIGSe.¹¹ Oxygen content gradient was observed due to inherent inhomogeneity in pulsed laser deposition (PLD) of SnO₂. 12 Varying oxygen content in thin films made by molecular beam epitaxy (MBE) was obtained by orienting vanadium metal and oxygen rich vanadium oxide sources opposite to each other.¹³ These studies demonstrate the importance of a vapor phase gradient as a parameter in high throughput experiments.

In radio frequency sputtering (RF sputtering), typically the sputtering chamber atmosphere is assumed uniform; thus, combinatorial gradients of different process gases are usually not studied. However, in noncombinatorial literature, it is known that inhomogeneity of thin films can be introduced at different substrate positions because of different gaseous particle bombardment energies, 14,15 as in the case of negative oxygen ions. It is also known that the film gradients can be introduced by the different mean free path and resulting reactivity of gaseous precursors, 16,17 such as atomic nitrogen

Received: March 9, 2018 Revised: April 18, 2018 Published: May 17, 2018



[†]Department of Materials Science, Fudan University, Shanghai 200433, China

^{*}Materials Science Center, National Renewable Energy Laboratory, Golden, Colorado 80401, United States

[§]Department of Physics, Oregon State University, Corvallis, Oregon 97330, United States

Department of Mechanical Engineering, University of Colorado at Boulder, Boulder, Colorado 80309, United States

¹Department of Metallurgical and Materials Engineering, Colorado School of Mines, Golden, Colorado 80401, United States

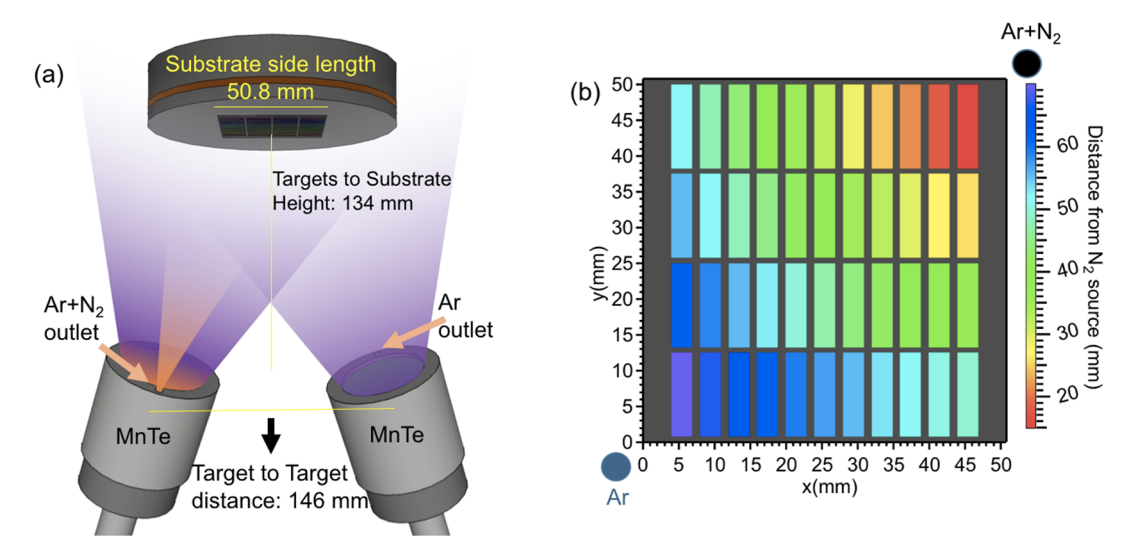


Figure 1. (a) Illustration of the combinatorial sputtering method used to create nitrogen gradient in thin film sample library. Two identical MnTe sputtering targets are set up opposing each other, one receiving Ar as sputtering gas, while the other one receiving both Ar and N_2 through gas outlets that are on the opposite side of each gun shield. The square substrate is placed above, such that a thin film material library is produced. (b) A grid of 44 points on the sample is established for spatially resolved characterization. The distance of each point between the nitrogen source increases from top right to bottom left along the sample diagonal. The distance from the nitrogen source in this work is defined as the distance from the intersection of substrate plane and the extrapolation of the Ar + N_2 gas pipe.

plasma versus molecular nitrogen plasma. Various gases such as oxygen, nitrogen, hydrogen, and halogens, are also frequently used for doping in sputtering, ¹⁸⁻²¹ indicating the importance to investigate the gas phase influence on resulting films. For sputtering experiments, the gas atmosphere may not be uniform in the chamber, especially for modern sputtering cathodes, where there is an option to supply gas close to the target surface.^{22,23} Thus, more attention should be paid to the relative position of the gas sources and its ability to influence the overall film properties.

Here, we determine nitrogen content in a combinatorial sample library as a function of the distance from the nitrogen source. Two identical sputtering cathodes loaded with MnTe targets are placed opposite to one another. The sputtering gas used to maintain plasma on each target is different, where one gun utilizes only argon and the other a combination of nitrogen and argon. We find that the nitrogen content in the thin film is higher, and the corresponding effect on the film is stronger, at substrate positions closer to the nitrogen source. The results of this work indicate that gradients of gaseous elements can influence the film properties and be applied as a combinatorial variable, expanding the scope of high-throughput experimental methods. This new understanding should allow for better control of composition from gaseous species and vapor phase effects during PVD syntheses.

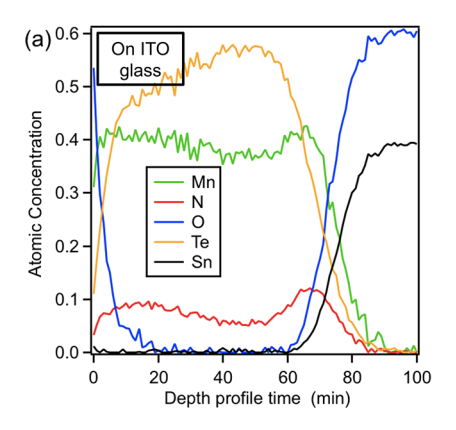
EXPERIMENTAL DETAILS

All thin film libraries presented in this work were synthesized in a combinatorial physical vapor deposition system AJA Orion 8 described in previous work. 24,25 As illustrated in Figure 1a, two MnTe targets were placed at an incident angel of 18° relative to the normal vector of the substrate surface, with the target-substrate height of 134 mm. Processing ultrahigh purity gases were introduced through a single port on each cathode shield. One sputtering source is plumbed to argon only, while the other source provides a mixture of argon and nitrogen. As plasma is generated around the target surface, a nitrogen-rich plasma exists near one gun and a nitrogen-poor plasma near the

other. This geometry modifies the surface of the MnTe target near the nitrogen outlet, contributing to nitrogen incorporation in the portion of the thin film nearest this source. The mixed Ar + N_2 source was plumbed through a pipe parallel to one of the MnTe sputter cathodes. The outlet was in the same plane as the target surface, as shown in Figure 1a. The color map in Figure 1b shows the distance of each sample point from the nitrogen source. The distance from nitrogen source in this work is defined as the distance from the intersection of substrate plane and the extrapolation of the Ar + N_2 gas pipe.

The total flow rate of Ar is 16 SCCM split between four cathode gas outlets (2 are unused), while nitrogen is supplied to a single gun only, with a flow rate of 1 and 2 SCCM. All results below are based on syntheses using a 2 SCCM nitrogen flow unless specified otherwise. The total operating pressure was kept at 3×10^{-3} Torr, and the base pressure of the chamber was around 5×10^{-7} Torr. Quartz substrates (50.8) mm square) were used to avoid impurities that could cause noise in compositional measurements. Each 50 mm circular sputtering cathode was held at a power of 40 W (2 W/cm²) after a 5 nm ZnTe buffer layer was deposited from another cathode. In an effort to mitigate charging effects in the Auger Electron Spectroscopy (AES) measurements, identical samples were produced on indium-tin-oxide-coated (ITO) Corning Eagle XG glass purchased from Delta Technologies, Ltd. The back side of each substrate was pasted with silver paint ("Leitsilber" by Ted Pella) to a sample platen to promote efficient heating and uniform substrate temperatures while the sample platen is heated by a SiC-based resistive heater. The substrate temperature was 300 °C for all depositions. The thickness of all the samples ranges from 200 to 300 nm as a function of the distance to the nitrogen source as shown in Figure S3. This thickness gradient is probably due to the fact that the poisoning of MnTe target by nitrogen can reduce the deposition rate.

The resulting thin film library is characterized at four rows with 12.5 mm spacing and 11 columns with 4 mm spacing. For these spatially resolved characterization, a predefined map is



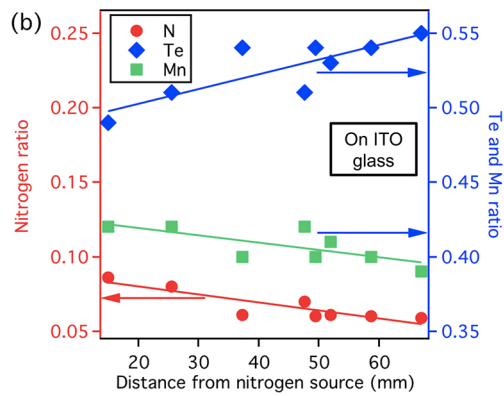


Figure 2. (a) Depth profile of atomic concentrations of the sample on ITO glass that is closest to the nitrogen source as measured by AES. The oxygen signal near the surface is likely due to the surface oxidation in the air. (b) Nitrogen, manganese, Tellurium fraction in the samples on ITO glass as a function of position on the sample library. It is obvious that nitrogen fraction is higher near the nitrogen source and vice versa for tellurium fraction.

programmed for all measurements. X-ray diffraction (XRD) to determine crystal structure was performed on a Bruker D8 Advance using Cu K α (λ = 1.54 Å) radiation and a high-resolution 2D detector. Composition was determined using X-ray fluorescence (XRF) on a Fischer XDV-SDD with a Ru X-ray source. Custom four point probe and sheet resistivity measurement systems built in-house utilized a Keithley source and voltage meter to control current and measure voltage. ²⁶ UV-vis spectroscopy was performed on a custom spectrometer using fibers and detectors from Ocean Optics scanning a range of 300–1000 nm. Further details about these spatially resolved characterization techniques have been published elsewhere. ^{27,28}

Single-point measurements were applied to specific points on samples in order to collect more detailed information on nitrogen content in the films. A JEOL 6320F field-emission scanning electron microscope (FE-SEM) using Thermo Fisher Pathfinder EDX software was operated with lower energy settings to maximize light element detection. Film compositions were also analyzed using Auger electron spectroscopy. In these measurements, a grid of depth profiles was performed using a script (Reference Physical Electronics SmartSoft v 4.4.1.7 control and acquisition software) that drove the sample manipulator, an argon ion gun, and spectral data acquisition. A 5 kV, 20 nA primary beam was used for analysis and sputter depth profiling was conducted using a 3 kV beam of Ar+. Direct spectra were numerically differentiated and analyzed as described previously.²⁹ Elemental compositions for each depth profile were determined using standard elemental sensitivity factors, integrated over depth, and composition normalized to 100%. The massive amount of data generated by each measurement was analyzed by customized procedures in Igor Pro. The data will be made available through the High Throughput Experimental Materials Database (HTEM) at https://htem.nrel.gov.³⁰

RESULTS AND DISCUSSION

We choose MnTe to investigate the effect of nitrogen gradients on the samples, and explore the dependence of nitrogen content on relative distance from the nitrogen source. MnTe was chosen for several reasons. MnTe has long been investigated as a traditional semiconductor and plays an important role in alloying with other chalcogenide semiconductors. It is predicted that nitrogen doping in MnTe is unfavorable due to the formation of MnN_x secondary phases. 33

For the purpose of this study, the secondary phase MnN_x would be an obvious indication of Nitrogen content in MnTe thin films, since the change in XRD or optoelectronic properties induced by MnN_x can be easily detected. In addition, N is supposed to substitute for Te, since compounds of Te and N are unstable. This is expected to lead to a deviation of Mn/Te ratio from unity, which can be easily measured. Thus, nitrogen substituted MnTe samples have been prepared to test the effect of nitrogen addition on the sample phase content, and its dependence on relative position from nitrogen source.

Figure 2a shows the atomic concentrations in a N-containing MnTe sample on ITO glass nearest to the nitrogen source, as a function of the depth profiling time in AES. Nitrogen content through the thickness of the film is not uniform, with slight accumulation close to the substrate. The sharp increase of oxygen at the zero sputtering time implies the oxidation near the surface. This oxidation is assumed to come from the long exposure time in the air. The oxidation in the deposition seems unlikely since the base pressure can be as low as 5×10^{-7} Torr and the oxidation only appears at the surface.

Figure 2b shows atomic concentrations for 8 points across the surface of the sample library deposited on ITO glass, as determined by integrating AES depth profiles. Nitrogen content clearly decreases from 0.086 to 0.059 as distance from the nitrogen source increases. At the same time, the tellurium content increases from 0.49 to 0.55, and manganese content decreases slightly as a result of the substitution of Te by N in the film. The decrease of Mn with increasing distance from the N₂ suggests the presence of Mn₃N₂, a more Mn-rich compound than MnTe, near the N₂ source. Generally, nitrogen is believed to substitute Te in II–VI compounds, and at high concentration may form metal-nitride compounds. ^{33,34}

To obtain composition results for all 44 points on the sample map, we used a combination of low-throughput AES/EDX results and high-throughput XRF measurements. To quantify nitrogen content of the remaining points, we used the ratio of heavier metallic elements, which is easily obtained from simpler methods such as XRF, as an input data. This in turn required establishing quantitative relationship between the metal composition and the nitrogen content from the samples where they were measured. For these calculations, we assume that all atoms in the film follow charge conservation laws, that

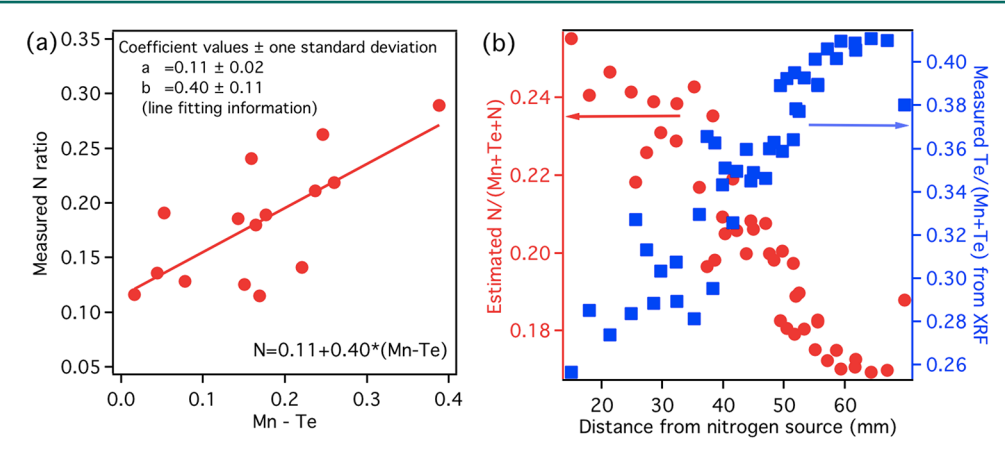


Figure 3. (a) N^{EDX} content as a function of $(Mn^{EDX} - Te^{EDX})$ from EDX measurements on a few samples. The line is the fitting relationship, and the points are measured values. (b) Estimated N based on EDX/XRF and $Te^{XRF}/(Mn^{XRF} + Te^{XRF})$ obtained by XRF for one sample library. Estimated N decreases with increasing distance from nitrogen source, while $Te^{XRF}/(Mn^{XRF} + Te^{XRF})$ increases.

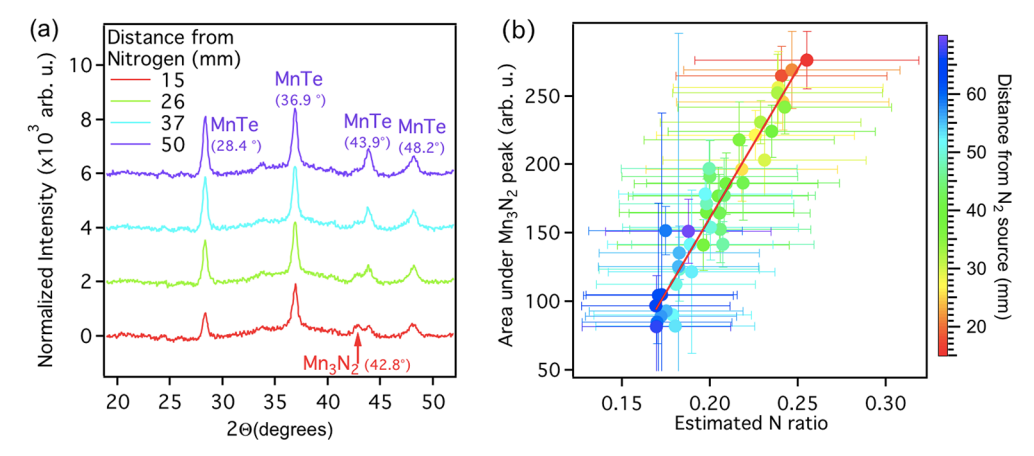


Figure 4. (a) XRD patterns of different points with different distances from nitrogen source. At these high nitrogen contents the Mn_3N_2 secondary phase is introduced. (b) Area under Mn_3N_2 peak (42.8°) as a function of distance from the nitrogen source. The nitrogen induced Mn_3N_2 phase increases with decreasing distance from the nitrogen source, as nitrogen content in the film increases.

is, that Mn^{2+} is bonded with Te^{2-} , and that remaining Mn^{2+} is bonded with nitrogen.

Figure 3a shows the N^{EDX} as a function of $(Mn^{EDX} - Te^{EDX})$ from EDX results for films deposited with nitrogen flow rate of 1 and 2 SCCM. Detailed N^{EDX} , Mn^{EDX} , Te^{EDX} data are summarized in Table S1. The points represent measured values, and the large scatter of the points originates from the intrinsic measurement difficulty of nitrogen via EDX. However, we have some confidence in the overall trend because it correlates well with the expected trend in the XRD patterns shown later. Therefore, the line fits were performed to get the relationship between N^{EDX} and $(Mn^{EDX} - Te^{EDX})$:

$$N^{EDX} = 0.11 + 0.40 \times (Mn^{EDX} - Te^{EDX})$$
 (1)

Since only N^{EDX} , Mn^{EDX} , Te^{EDX} are present in the sample, the sum of their atomic fractions is set to 1

$$N^{EDX} + Mn^{EDX} + Te^{EDX} = 1$$
 (2)

In addition, Mn^{XRF}/Te^{XRF} can be also be obtained from XRF. Assuming that the metal ratios in both XRF and EDX are the same

$$Mn^{EDX}/Te^{EDX} \approx Mn^{XRF}/Te^{XRF}$$
 (3)

one can use three equations (eqs 1–3) with three unknowns (N^{EDX} , Mn^{EDX} , Te^{EDX}) to estimate the nitrogen content from the measured Mn^{XRF} and Te^{XRF} values.

We note that this is just an estimate of the nitrogen content, because the standard deviation of the slope in eq 1 is quite large (25%) because of the difficulty in measurement of nitrogen in EDX. To get higher confidence in these results, we repeated this analysis procedure using AES data, denoted as N^{AUG} and $(Mn^{AUG}-Te^{AUG}).$ The fit obtained can be described as N^{AUG} = 0.1 + 0.3 \times (Mn $^{AUG}-Te^{AUG})$, shown in Figure S1. This is very similar to the relationship derived in eq 1, with the difference in slope that may result from the Mn/Te measurement uncertainty in AES. Estimated N from both equations (from Auger and EDX data) are compared in Figure S2, which shows that they share similar trends with slightly different values, increasing the confidence in our analysis procedure.

Figure 3b shows the result of estimated N and measured $Te^{XRF}/(Mn^{XRF} + Te^{XRF})$ ratio for all samples in one library. As a comparison, when both sputtering guns used only Ar as a process gas with all other parameters being the same, $Te^{XRF}/(Mn^{XRF} + Te^{XRF})$ ratio was uniform around 0.5. However, when nitrogen is plumbed to one of the sputtering guns, $Te^{XRF}/(Mn^{XRF} + Te^{XRF})$ is below 0.42. Moreover, the $Te^{XRF}/(Mn^{XRF} + Te^{XRF})$ ratio increases with increasing distance from the

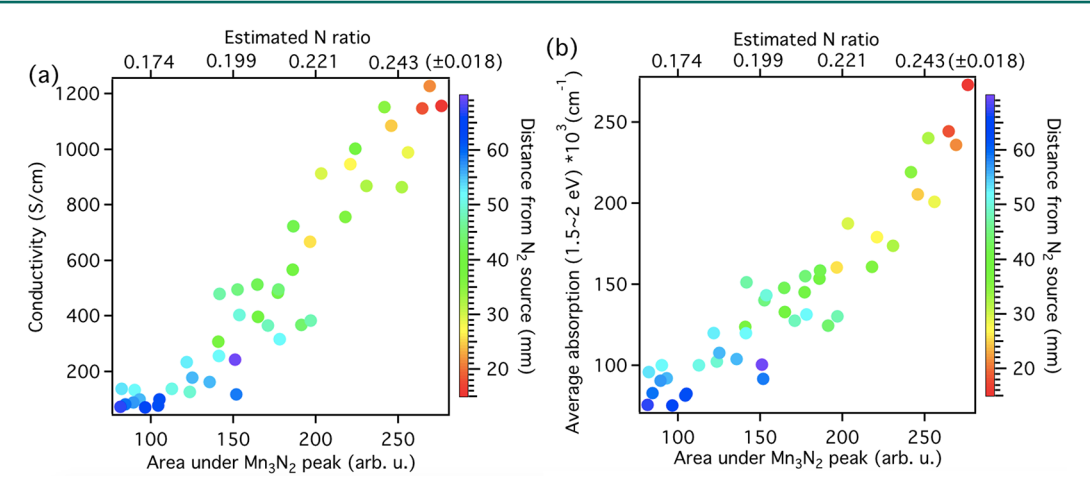


Figure 5. (a) Electrical conductivity and (b) average optical absorption from 1.5 to 2 eV as a function of area under Mn_3N_2 peak and nitrogen content, with distance from N_2 source as a color scale. Conductivity and absorption increase as the estimated nitrogen content and the area under Mn_3N_2 increase.

nitrogen source, indicating the presence of nitrogen in the areas closer to the nitrogen source. The estimated nitrogen from EDX/XRF calibration decreases from 0.26 to 0.17 with increasing distance from the nitrogen source. Similarly, the estimated N from Auger/XRF calibration shows the same trend as a function of distance, but with lower overall N values (0.129-0.137), and higher Te/(Mn + Te) ratios (0.461-0.472). This result shows the suitability of this method in determining a gradient in nitrogen content.

Introduction of nitrogen into MnTe also causes the crystal structure to change, illustrating the importance of a controlled gas ambient environment in PVD. Figure 4a shows the XRD patterns of four points of a library, with distance from the nitrogen source 15, 26, 37, and 50 mm, respectively. All films show the NC (Nickeline) phase of MnTe with one small peak attributed to Mn₃N₂. It is not unexpected that nitrogen in the film can induce a manganese nitride secondary phase at high concentration, in addition to serving as a dopant at low concentration. The noisy XRD patterns here mainly come from the intrinsic poor crystallinity caused by nitride impurities. It should be noted from Figure 4a that MnTe peaks decreases as the Mn₃N₂ increases but without any measurable shift in position. This indicates the decrease of the MnTe crystallinity induced by the presence of Mn₃N₂. While the Mn₃N₂ peak is small, Figure 4b shows the area under that peak (at 42.8°) increases as estimated nitrogen increases, again suggesting the validity of the calculation method used above. The error bars for the area are seemingly large, but the trend is clear due to combinatorial character of our method. The error of the estimated N ratio mainly comes from the fitting deviations (25%) in the EDX measurement results (Figure 3a). The color scale of each point gives the distance of the measured point on the thin film from N_2 source.

Optical and electrical properties also vary across the library (Figure 5). To determine if the gradient of conductivity and absorption is related to nitrogen, we correlated these optoelectronic properties with the nitrogen content and with the area under Mn₃N₂ peak. Since the area under impurity peak is linearly related to estimated N content (see fits in Figure 4b), these two quantities are plotted as bottom and top axis of Figure 5. As shown in Figure 5a, the conductivity of the sample libraries increases with increasing Mn₃N₂ peak area (bottom axis) and the corresponding nitrogen content (top axis). This

increase in conductivity can be explained by the high conductivity of manganese nitride compounds (~200 S/cm for MnN_x deposited at 100 °C) compared to the MnTe compound (~10 S/cm for pure nickeline phase deposited at 300 °C). Figure 5b depicts the average absorption in the 1.5-2.0 eV spectral range as a function of impurity peak area and the nitrogen content. We can attribute the observed increase in absorption to the appearance of Mn₃N₂ phase, because pure NC-MnTe shows an average absorption of 5×10^4 cm⁻¹, whereas the MnN_a compound shows a higher absorption of 3 × 10^{5} in the same range (1.5–2.0 eV). Generally, these changes of the optoelectronic properties verified the motivation for the choice of MnTe for this study, that the nitrogen doping in MnTe would result in the secondary MnN_x phase that can be easily detected. The optical and electrical property changes correlate well with the nitrogen content gradient, confirming the success of this method of inducing nitrogen gradients in the

Finally, we discuss our results in the context of the previous studies on the combinatorial gradient of oxygen content in PLD and MBE. 12,13 In PLD, the oxygen gradient originates from inhomogeneity of the plasma plume, which is difficult to control and may be inherent only to this technique. In MBE, there is a more controlled oxygen content gradient, but this requires two sources that have multivalent transition metal states, which may not be applicable to the single valent main group metals. In the sputtering experiment described here, nitrogen gradient can be controlled, because it is introduced by the gas outlet rather than coming from compounds, which also expands the application of this method to more material systems. In addition, we note that sputtering is a very different deposition technique compared to PLD and MBE because of the presence of an electric field and the resulting unique plasma kinetics. Thus, more detailed investigations are warranted to further explore its potential in generating combinatorial gas content, and to study the kinetic energy of the reactive gas species as a function of distance from the target.

SUMMARY

In summary, we demonstrated a simple cosputtering configuration that can obtain a combinatorial gradient of gaseous element content in a thin film sample library. The nitrogen gradient was achieved by using two opposing sputter

cathodes loaded with MnTe targets, one connected to pure Ar gas and the other connected to a mixture of Ar and N₂. The MnTe is chosen since the nitrogen coordination effect in MnTe can be easily measured. It was found that nitrogen gradients in thin films can be achieved, correlating with the distance from the nitrogen source, with the higher content closer to the source of nitrogen. The nitrogen content changes the crystal structure and the phase content of the material from MnTe, to MnTe with Mn₃N₂ secondary phase. The optoelectronic properties of the resulting thin film sample libraries also change as a function of the nitrogen content or the crystal structure, further confirming the nitrogen gradient along the substrate. The results of this work demonstrate the gradient of gaseous elements in sputtered thin films, which has a potential to expand the range of applications of combinatorial methods.

ASSOCIATED CONTENT

S Supporting Information

The Supporting Information is available free of charge on the ACS Publications website at DOI: 10.1021/acscombsci.8b00035.

Nitrogen, Mn, and Te ratio measured from EDX; N as a function of (Mn–Te) from Auger; comparison of estimated N based on actual Auger and EDX data; and thickness information for all the 44 points (PDF)

AUTHOR INFORMATION

Corresponding Authors

*E-mail: ybhan14@fudan.edu.cn. *E-mail: Andriy.Zakutayev@nrel.gov.

ORCID ®

Yanbing Han: 0000-0003-1159-1005 Craig Perkins: 0000-0002-9036-8698 Andriy Zakutayev: 0000-0002-3054-5525

Notes

The authors declare no competing financial interest.

■ ACKNOWLEDGMENTS

This work was supported by the US Department of Energy, Office of Science, Basic Energy Sciences, as part of the Energy Frontier Research Center "Center for Next Generation of Materials by Design" under contract No. DE-AC36-08GO28308 to Alliance for Sustainable Energy, LLC, the manager and operator of the National Renewable Energy Laboratory. Y.H. was supported from Science and Technology Commission of Shanghai Municipality (No. 16JC1400603) and a grant from the National Natural Science Foundation of China (No. 61471126). Y.H. also appreciated the stipend from China Scholarship Council. K.R.T. was supported by the US National Science Foundation (DMREF-1534503). The authors thank Bobby To for the EDX measurement. The U.S. Government retains a nonexclusive, paid-up, irrevocable, worldwide license to publish or reproduce the published form of this work, or allow others to do so, for U.S. Government purposes.

REFERENCES

- (1) Green, M. L.; Takeuchi, I.; Hattrick-Simpers, J. R. Applications of High Throughput (Combinatorial) Methodologies to Electronic, Magnetic, Optical, and Energy-Related Materials. *J. Appl. Phys.* **2013**, *113* (23), 231101.
- (2) Green, M. L.; Choi, C. L.; Hattrick-Simpers, J. R.; Joshi, A. M.; Takeuchi, I.; Barron, S. C.; Campo, E.; Chiang, T.; Empedocles, S.;

Gregoire, J. M.; et al. Fulfilling the Promise of the Materials Genome Initiative with High-Throughput Experimental Methodologies. *Appl. Phys. Rev.* **2017**, *4* (1), 011105.

- (3) Potyrailo, R.; Rajan, K.; Stoewe, K.; Takeuchi, I.; Chisholm, B.; Lam, H. Combinatorial and High-Throughput Screening of Materials Libraries: Review of State of the Art. ACS Comb. Sci. 2011, 13 (6), 579–633
- (4) Han, Y.; Siol, S.; Zhang, Q.; Zakutayev, A. Optoelectronic Properties of Strontium and Barium Copper Sulfides Prepared by Combinatorial Sputtering. *Chem. Mater.* **2017**, 29 (19), 8239–8248.
- (5) Decker, P.; Naujoks, D.; Langenkämper, D.; Somsen, C.; Ludwig, A. High-Throughput Structural and Functional Characterization of the Thin Film Materials System Ni–Co–Al. ACS Comb. Sci. 2017, 19 (10), 618–624.
- (6) Siol, S.; Dhakal, T. P.; Gudavalli, G. S.; Rajbhandari, P. P.; Dehart, C.; Baranowski, L. L.; Zakutayev, A. Combinatorial Reactive Sputtering of In2S3 as an Alternative Contact Layer for Thin Film Solar Cells. ACS Appl. Mater. Interfaces 2016, 8 (22), 14004–14011.
- (7) Stein, H.; Naujoks, D.; Grochla, D.; Khare, C.; Gutkowski, R.; Grützke, S.; Schuhmann, W.; Ludwig, A. A Structure Zone Diagram Obtained by Simultaneous Deposition on a Novel Step Heater: A Case Study for Cu2O Thin Films. *Phys. Status Solidi A* **2015**, *212* (12), 2798–2804.
- (8) Siol, S.; Schulz, P.; Young, M.; Borup, K. A.; Teeter, G.; Zakutayev, A. Combinatorial in Situ Photoelectron Spectroscopy Investigation of Sb2Se3/ZnS Heterointerfaces. *Adv. Mater. Interfaces* **2016**, *3* (24), 1600755.
- (9) Sreenivasan, R.; Adomaitis, R. A.; Rubloff, G. W. A Comparative Study of Reactor Designs for the Production of Graded Films with Applications to Combinatorial CVD. *J. Cryst. Growth* **2008**, *310* (2), 270–283.
- (10) Kafizas, A.; Hyett, G.; Parkin, I. P. Combinatorial Atmospheric Pressure Chemical Vapour Deposition (cAPCVD) of a Mixed Vanadium Oxide and Vanadium Oxynitride Thin Film. *J. Mater. Chem.* **2009**, *19* (10), 1399.
- (11) Colombara, D.; Berner, U.; Ciccioli, A.; Malaquias, J. C.; Bertram, T.; Crossay, A.; Schöneich, M.; Meadows, H. J.; Regesch, D.; Delsante, S.; et al. Deliberate and Accidental Gas-Phase Alkali Doping of Chalcogenide Semiconductors: Cu (In, Ga) Se 2. Sci. Rep. 2017, 7, 43266.
- (12) Keller, D. A.; Barad, H.-N.; Rietwyk, K. J.; Ginsburg, A.; Borvick, E.; Priel, M.; Anderson, A. Y.; Meir, S.; Zaban, A. Oxygen Concentration as a Combinatorial Parameter: The Effect of Continuous Oxygen Vacancy Variation on SnO 2 Layer Conductivity. *Mater. Chem. Phys.* **2018**, 208, 289–293.
- (13) Zhang, H.-T.; Zhang, L.; Mukherjee, D.; Zheng, Y.-X.; Haislmaier, R. C.; Alem, N.; Engel-Herbert, R. Wafer-Scale Growth of VO 2 Thin Films Using a Combinatorial Approach. *Nat. Commun.* 2015, 6, 8475
- (14) Ichihara, K.; Inoue, N.; Okubo, M.; Yasuda, N. The Origin of the Inhomogeneity of Electrical Resistivity in Magnetron-Sputtered Indium Tin Oxide Thin Films. *Thin Solid Films* **1994**, 245 (1–2), 152–156.
- (15) Herrmann, D.; Oertel, M.; Menner, R.; Powalla, M. Analysis of Relevant Plasma Parameters for ZnO: Al Film Deposition Based on Data from Reactive and Non-Reactive DC Magnetron Sputtering. *Surf. Coat. Technol.* **2003**, 174-175, 229–234.
- (16) Caskey, C. M.; Richards, R. M.; Ginley, D. S.; Zakutayev, A. Thin Film Synthesis and Properties of Copper Nitride, a Metastable Semiconductor. *Mater. Horiz.* **2014**, *1* (4), 424–430.
- (17) Caskey, C. M.; Holder, A.; Shulda, S.; Christensen, S. T.; Diercks, D.; Schwartz, C. P.; Biagioni, D.; Nordlund, D.; Kukliansky, A.; Natan, A.; et al. Synthesis of a Mixed-Valent Tin Nitride and Considerations of Its Possible Crystal Structures. *J. Chem. Phys.* **2016**, 144 (14), 144201.
- (18) Yamaguchi, T.; Matsufusa, J.; Kabasawa, H.; Yoshida, A. Thin Films of CuInSe2 Produced by RF Sputtering with Intentional Oxygen Doping. *J. Appl. Phys.* **1991**, *69* (11), 7714–7719.

(19) Wei, D.; Liu, Y.; Wang, Y.; Zhang, H.; Huang, L.; Yu, G. Synthesis of N-Doped Graphene by Chemical Vapor Deposition and Its Electrical Properties. *Nano Lett.* **2009**, *9* (5), 1752–1758.

- (20) Fioretti, A. N.; Stokes, A.; Young, M. R.; Gorman, B.; Toberer, E. S.; Tamboli, A. C.; Zakutayev, A. Effects of Hydrogen on Acceptor Activation in Ternary Nitride Semiconductors. *Adv. Electron. Mater.* **2017**, 3 (3), 1600544.
- (21) Ho, E.; Fisher, P. A.; House, J. L.; Petrich, G. S.; Kolodziejski, L. A.; Walker, J.; Johnson, N. M. Hydrogen Passivation in Nitrogen and Chlorine-doped ZnSe Films Grown by Gas Source Molecular Beam Epitaxy. *Appl. Phys. Lett.* **1995**, *66* (9), 1062–1064.
- (22) Huo, C.; Lundin, D.; Raadu, M. A.; Anders, A.; Gudmundsson, J. T.; Brenning, N. On the Road to Self-Sputtering in High Power Impulse Magnetron Sputtering: Particle Balance and Discharge Characteristics. *Plasma Sources Sci. Technol.* **2014**, 23 (2), 025017.
- (23) Jäger, T.; Bissig, B.; Döbeli, M.; Tiwari, A. N.; Romanyuk, Y. E. Thin Films of SnO2: F by Reactive Magnetron Sputtering with Rapid Thermal Post-Annealing. *Thin Solid Films* **2014**, 553, 21–25.
- (24) Welch, A. W.; Baranowski, L. L.; Zawadzki, P.; DeHart, C.; Johnston, S.; Lany, S.; Wolden, C. A.; Zakutayev, A. Accelerated Development of CuSbS2 Thin Film Photovoltaic Device Prototypes. *Prog. Photovoltaics* **2016**, 24 (7), 929–939.
- (25) Welch, A. W.; Baranowski, L. L.; Peng, H.; Hempel, H.; Eichberger, R.; Unold, T.; Lany, S.; Wolden, C.; Zakutayev, A. Trade-Offs in Thin Film Solar Cells with Layered Chalcostibite Photovoltaic Absorbers. *Adv. Energy Mater.* **2017**, *7* (11), 1601935.
- (26) Zakutayev, A.; Luciano, F. J., IV; Bollinger, V. P.; Sigdel, A. K.; Ndione, P. F.; Perkins, J. D.; Berry, J. J.; Parilla, P. A.; Ginley, D. S. Development and Application of an Instrument for Spatially Resolved Seebeck Coefficient Measurements. *Rev. Sci. Instrum.* **2013**, *84* (5), 053905.
- (27) Peng, H.; Ndione, P. F.; Ginley, D. S.; Zakutayev, A.; Lany, S. Design of Semiconducting Tetrahedral Mn 1– X Zn X O Alloys and Their Application to Solar Water Splitting. *Phys. Rev. X* **2015**, 5 (2), 021016.
- (28) Caskey, C. M.; Seabold, J. A.; Stevanović, V.; Ma, M.; Smith, W. A.; Ginley, D. S.; Neale, N. R.; Richards, R. M.; Lany, S.; Zakutayev, A. Semiconducting Properties of Spinel Tin Nitride and Other IV 3 N 4 Polymorphs. *J. Mater. Chem. C* **2015**, 3 (6), 1389–1396.
- (29) Repins, I.; Contreras, M. A.; Egaas, B.; DeHart, C.; Scharf, J.; Perkins, C. L.; To, B.; Noufi, R. 19. 9%-efficient ZnO/CdS/CuInGaSe2 Solar Cell with 81. 2% Fill Factor. *Prog. Photovoltaics* **2008**, *16* (3), 235–239.
- (30) Zakutayev, A.; Wunder, N.; Schwarting, M.; Perkins, J. D.; White, R.; Munch, K.; Tumas, W.; Phillips, C. An Open Experimental Database for Exploring Inorganic Materials. *Sci. Data* **2018**, *5*, 180053.
- (31) Wasscher, J. D. Electrical Transport Phenomena in MnTe, an Antiferromagnetic Semiconductor. PhD Thesis, Department of Applied Physics, Technische Hogeschool Eindhoven, Eindhoven, Netherlands, 1969. DOI: DOI: 10.6100/IR43336.
- (32) Ferrand, D.; Cibert, J.; Bourgognon, C.; Tatarenko, S.; Wasiela, A.; Fishman, G.; Bonanni, A.; Sitter, H.; Koleśnik, S.; Jaroszyński, J.; et al. Carrier-Induced Ferromagnetic Interactions in P-Doped Zn_(1-x)Mn_xTe Epilayers. *J. Cryst. Growth* **2000**, 214-215, 387–390.
- (33) Baron, T.; Saminadayar, K.; Magnea, N. Nitrogen Doping of Tellurium-Based II–VI Compounds during Growth by Molecular Beam Epitaxy. *Appl. Phys. Lett.* **1995**, *67* (1995), 2972.
- (34) Lee, K. S.; Oh, G.; Kim, E. K. Growth of P-Type ZnTe Thin Films by Using Nitrogen Doping during Pulsed Laser Deposition. *J. Korean Phys. Soc.* **2015**, *67* (4), *672–675*.